*Yang Zhou*
*Jiachuan Xu* ✉
*Weidong Qi*
*Xinyu Sun*
*Han Xu*

https://doi.org/10.21278/TOF.483060723
ISSN 1333-1124
eISSN 1849-1391

# OPTIMISED DESIGN OF FRAME TOPOLOGY BASED ON THE EXPONENTIAL SCALING HIERARCHY ANALYSIS METHOD

**Summary**

Relying on the research and development project of a specific company, the present study conducts a topology optimisation design for an aluminium alloy frame intended for a light-duty truck. In light of the discrepancy observed in the conventional strength calculation outcomes for the unconstrained frame, the inertia release method is employed to determine the strength of the said frame. A novel approach is presented to address the issue of multi-condition frame topology optimisation. The proposed method incorporates weighting coefficients to facilitate the optimisation process. The weight coefficients for each working condition are determined using the exponential scale hierarchical analysis method. Subsequently, an objective function is formulated for the multi-objective topology optimisation of an aluminium alloy frame. The proposed method aims to optimise the topology of an aluminium alloy frame by considering the constraints of volume fraction and the objective of minimising flexibility under various working conditions. The findings indicate that the optimised aluminium alloy frame exhibits an 18.9% increase in bending stiffness and a 150.3% increase in torsional stiffness. The safety coefficient of the frame strength exceeds 1 under all operational circumstances. The frame has a mass of 157 kg, which is reduced by 30.8%. The performance of the optimised frame is significantly enhanced, resulting in a noticeable lightweight effect.

*Key words:* *exponential scaling hierarchy analysis; inertia release method; topology optimisation; lightweighting; weighting factors*

## 1. Introduction

The frame of an automobile is a crucial component that serves as a platform for the installation of other systems. It is designed to withstand various loads encountered during the vehicle's operation. However, the mass of the frame is large, accounting for 20% to 40% of the total mass of the vehicle [1]. Relevant literature shows that for every 10% reduction in the total mass of a car, the fuel efficiency can be improved by 7% [2]. Relevant data from the European Aluminium Association shows that a 100 kg reduction in total vehicle mass can save 0.6 l of fuel per 100 km [3]. Since the lightweighting of the frame has a great impact on energy saving and emission reduction goals, it occupies an important position in the design of the whole vehicle.

Automotive lightweighting methods are mainly divided into three major parts, i.e., structural lightweighting, material lightweighting, and advanced production and manufacturing processes [4]. There are four main structural lightweighting methods, namely topology optimisation, shape optimisation, size optimisation, and morphology optimisation. Material lightweighting can be used to partially replace the raw material with aluminium alloy, advanced high-strength steel, carbon fibre, and so on. Advanced manufacturing processes mainly include laser welding, hot stamping and forming, aluminium alloy die casting, and so on. Among them, topology optimisation and aluminium alloy materials are widely used in automotive lightweight design.

Lai et al. [5] proposed a solid isotropic material penalty difference modelling method (SIMP) based on variable density topology optimisation for the main structure of a wall climbing robot, with a considerable lightweighting effect. Wang [6] proposed a multi-case collaborative topology optimisation approach for the lightweight design of a certain unmanned vehicle frame, and the resulting reconstructed frame was reduced by 124.5 kg compared to the original frame. Li et al. [7] determined the weight coefficients of the multi-conditional optimisation objective function by comparing the orthogonal design of the experiments method, the grey correlation analysis method, the entropy weight method, and the 1~9 scale hierarchy analysis method, and carried out a multi-objective topology optimisation design for the problem of the welded joints distribution of rail vehicles. The number of welded joints with a diameter of 6 mm was reduced by 17.8% after optimisation. Ma et al. [8] proposed to combine implicit parametric modelling with topology optimisation for the multi-objective optimisation of automotive subframes by the cross-section shape control method, resulting in a final lightweighting rate of 14.5%. The method can effectively reduce the number of variables in the design process, but the coupling phenomena between variables when dealing with complex parts can easily appear. The hierarchical analysis method can effectively address this issue.

Hierarchical analysis is a system analysis method that combines qualitative and quantitative methods, including the 1~9 scale, fractional scale, exponential scale, and other methods [9]. Among them, the exponential scaling method can effectively solve multi-objective complex decision-making problems due to its judgment matrix consistency and thinking consistency, its strong consistency matrix construction ability, and its good mathematical structure. Tao et al. [10] proposed a global assessment method for the security risk of Telematics, established a Telematics security risk assessment model through the exponential scale hierarchical analysis method, and proved the effectiveness of the assessment method through arithmetic examples. To address the problem of mudslide hazard assessment, Gao [11] proposed a fuzzy comprehensive evaluation model based on fuzzy hierarchical analysis, which effectively evaluated the hazard level of various types of mudslides. Sun et al. [12] proposed applying the exponential scale method to the assessment of the bridge technical condition, and the calculation results showed that the exponential scale more accurately reflects the importance of the relationship between the components of steel-tube concrete arch bridges than the 1~9 scale. Wang and Gan [13] proposed a model combining fuzzy theory and hierarchical analysis for assessing the survivability of warship propulsion systems in severe shock environments. The model is a fast and robust method to obtain the level of damage of each critical part of the propulsion system. Krstic et al. [14] proposed a methodology for assessing the safety level of aircraft performance by ranking multiple criteria using hierarchical analysis. Zhou et al. [15] proposed a non-dominated sequential genetic algorithm-analysis of the hierarchy (NSGA-AHP) method for decision-making and the analysis of multi-objective structural optimisation. The feasibility of the method is verified by establishing a multi-objective optimisation model and optimising the structure of a disc brake as an example.

Hierarchical analysis holds significant importance in numerous disciplines. However, there is a lack of research on the application of exponentially scaled hierarchical analysis for

frame lightweighting using multi-case topology optimisation. In this paper, we present a novel approach for achieving the lightweight design of a steel frame through the utilisation of a multi-case topology optimisation method with weight coefficients. The methodology employed in this study is founded on exponential scaling hierarchical analysis. The project was commissioned by a corporate entity with primary focus on investigating the use of aluminium alloy 6061 material for the purpose of designing lightweight truck frames, with the intention of replacing the current steel frames. Firstly, a preliminary finite element model of the steel frame is developed to examine its natural frequencies and stiffness properties. This model also serves as a reference for comparing the performance of the aluminium alloy frame. In the context of the unconstrained frame problem, the inertia release method is used to ascertain the structural integrity of the initial frame. The aforementioned calculation forms the basis for the subsequent design of topology optimisation. Since the 1~9 scale indicates the difference in importance between two factors, it can easily lead to problems such as the reversal of evaluation results and inconsistency between the judgment matrix and thinking consistency. This paper proposes the use of the exponential scale hierarchical analysis method to calculate the weight value of each working condition in the process of automobile driving, and to carry out the frame topology optimisation design. The topology optimisation results of the aluminium alloy frame were obtained after 23 iterations. Finally, the optimised aluminium alloy frame is subjected to the same finite element analysis as the original steel frame. The results suggest that the performance metrics of the aluminium alloy frame not only meet the applicable benchmarks but also exceed those of the original frame.

## 2. Performance Analysis of the Original Frame

### 2.1 Modelling of the Original Frame

**Table 1** Properties of Q345 material

| Material | Modulus of elasticity/(N/m$^2$) | Poisson ratio | Density/(kg/m$^3$) | Shear modulus/(N/m$^2$) | Yield strength/(N/m$^2$) |
|---|---|---|---|---|---|
| Q345 | 2.06E+11 | 0.28 | 7.85E+3 | 7.9E+10 | 3.45E+8 |

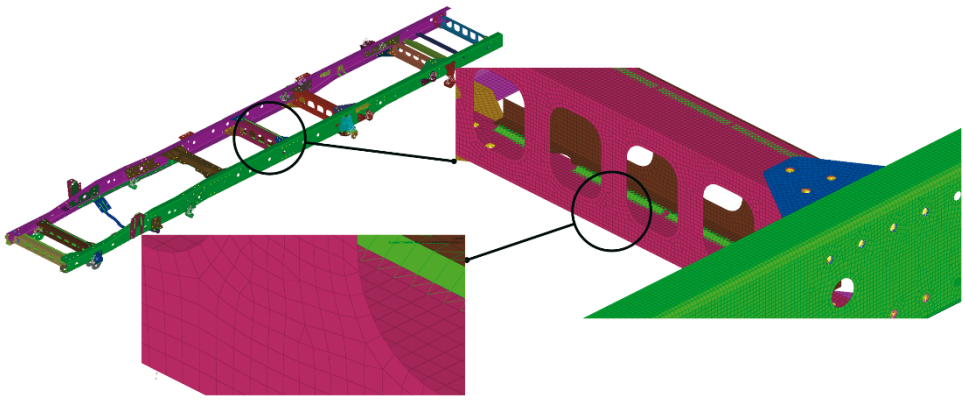

**Fig. 1** Finite element model of the original steel frame

The longitudinal beams of the original steel frame are in the form of grooves, and the longitudinal beams on both sides are connected by a number of cross beams in the centre. The front suspension is retrofitted with a torsion-resistant cross member, which is bolted to the longitudinal beams, and the reinforcing beams of the cross member are welded to the cross member. HyperMesh software was utilised to extract the midplane, remove fine chamfers, patch the full face, and give the frame the material properties as shown in Table 1. The frame mesh is mainly divided into a 5mm 2D mesh, and some parts that cannot be extracted from the

midplane due to the complex structure are meshed tetrahedrally according to their 3D models. The mesh consists mainly of triangles and quadrilaterals, while the solid mesh is tetrahedral. The total number of meshes is 386,564. The mesh connections refer to the physical connections of the frame, which encompass both bolted and welded connections. The bolted connections are established in HyperMesh using the bolt command, and the bolts are represented in the form of CBAR. The nodes at the edges of each bolt hole are connected to the centre point using RBE2 elements, and the centre points of two or more bolt holes are connected using CBAR beam elements to simulate the bolts. To assign properties to the CBAR unit, the Beamsection property of the beam unit is created. The section shape is set to ROD, and different radius values are defined by measuring the size of the bolt holes and selecting the corresponding properties when creating the bolt connections. The weld is created in HyperMesh using the seam command. The weld is simulated using the pentahedral cell and the RBE3 cell. The pentahedral cell simulates the weld, while the RBE3 cell connects the weld cell to the 2D cell. The final finite element model of the original steel frame is shown in Fig. 1.

## 2.2 Free Modal Analysis of the Original Frame

The light-duty truck engine studied in this paper is an inline four-cylinder diesel engine, with an idling speed of about 750 r/min and an idling vibration frequency of 25 Hz. The low-order intrinsic frequency of the original steel frame and the aluminium alloy frame obtained by subsequent design should avoid the engine idling frequency.

**Table 2** The first six orders of intrinsic frequency of the original steel frame

| Order | Steel frame intrinsic frequency /Hz |
|---|---|
| 1 | 6.71 |
| 2 | 20.03 |
| 3 | 25.16 |
| 4 | 33.78 |
| 5 | 35.67 |
| 6 | 54.78 |

The first six orders of free modal frequencies of the original steel frame are shown in Table 2. The results show that the first-order free mode frequency of the original steel frame is 6.71 Hz, which is located in the 2-8 Hz band of the roadway excitation frequency, and it is easy to resonate with the roadway, affecting the safety and durability of the frame. The third order intrinsic frequency in the low-order frequency is very close to the engine idling vibration frequency, and attention should be paid to the influence of engine idling on the safety of the frame. Therefore, the optimised first-order free mode should be greater than 10Hz and the low-order frequency should avoid the engine idling frequency.

## 2.3 Original Frame Stiffness Analysis

The frame bending stiffness is calculated as:

$$K_{bend} = \frac{1}{2}\left( \frac{F}{D_{\max l}} + \frac{F}{D_{\max r}} \right) \tag{1}$$

where $K_{bend}$ denotes the overall bending stiffness of the frame (N/mm), $F$ is the total load applied to the left and right longitudinal beams of the frame (N), and $D_{\max l}$ and $D_{\max r}$ denote the vertical displacements of the left and right longitudinal beam, respectively, at the point of load application (mm).

The frame torsional stiffness is calculated as:

$$K_{tor} = \frac{M_t}{\gamma_t} = \frac{F_t \times L}{\gamma_t} \tag{2}$$

where $K_{tor}$ is the torsional stiffness of the frame (N·mm/°), $M_t$ is the applied torsional moment (N·mm), $F_t$ is the size of the unilateral load on which the frame torsion occurs (N), $L$ is the distance between the two sides of the load (mm), and $\gamma_t$ is the torsional angle of the frame (°).

Constraints, as depicted in Table 3, are implemented on the frame model, where X, Y, and Z represent the degrees of freedom in the translational direction, respectively. The established load constraints for the bending and torsional stiffness of the original steel frame are depicted in Fig. 2. According to the stiffness calculation formula, stiffness is defined as the ratio of the load to the corresponding deformation, indicating the frame's ability to resist recoverable deformation. The stiffness can be determined by inputting the required load into the HyperMesh software, calculating the corresponding deformation, and verifying the elastic deformation of the frame. In this paper, the load size is taken as 1000 N. The displacement cloud and the displacement magnitude (unit: mm) at the load obtained by HyperMesh software are shown in Fig. 3. In the figure, the frame displacement transition is smooth, without obvious distortion, and the overall frame displacement is reasonable. The calculated bending stiffness of the original steel frame is $K_{bend}$ =1060.43 N/mm, while the torsional stiffness is $K_{tor}$ =198373.87 N·mm/°.

**Table 3** Original frame stiffness analysis constraints

| | | | | | |
|---|---|---|---|---|---|
| Bending stiffness | Binding position | Left front wheel | Right front wheel | Left rear wheel | Right rear wheel |
| | Constraint freedom | Z | Z | X, Z | X, Y, Z |
| Torsional stiffness | Binding position | Midpoint of front-end cross member | Left rear wheel | Right rear wheel | -- |
| | Constraint freedom | Z | X, Z | X, Y, Z | -- |

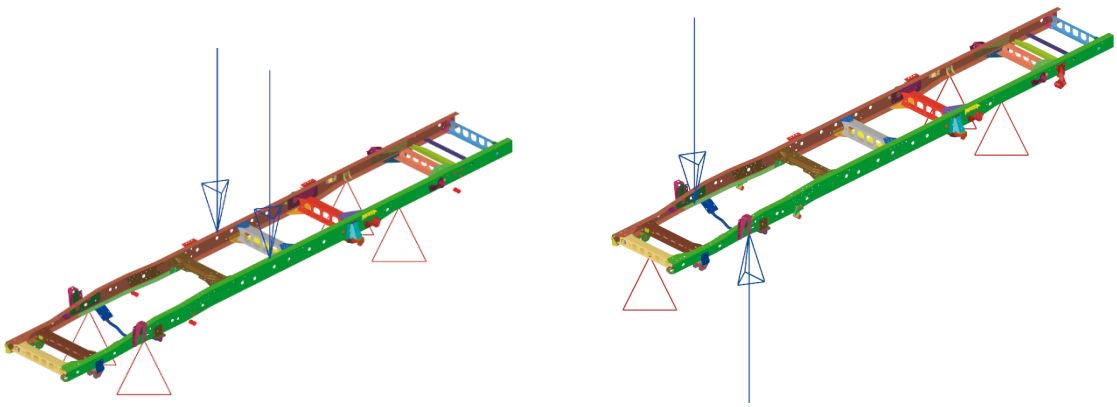

(a) Bending stiffness (b) Torsional stiffness

**Fig. 2** Original frame stiffness analysis loads and constraints

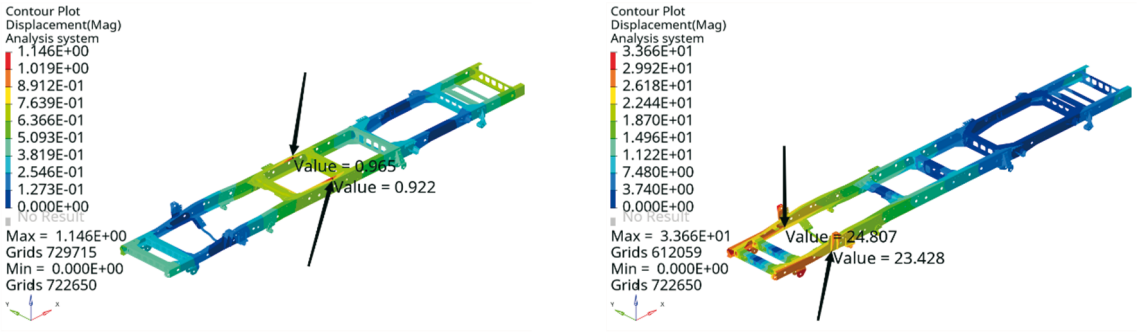


(a) Bending stiffness (b) Torsional stiffness

**Fig. 3** Displacement cloud of the original frame stiffness analysis

**Table 4** Frame performance indicators

| Performance metrics | Performance indicator values |
|---|---|
| First order intrinsic frequency | >10 Hz |
| Other intrinsic frequencies | Avoid the engine idling frequency of 25 Hz. |
| Bending stiffness | >1055.41 N/mm |
| Torsional stiffness | >198373.87 N·mm/° |

In order to make the performance of the subsequent lightweight-designed aluminium alloy frame no lower than that of the original steel frame, the optimised performance benchmarking indexes shown in Table 4 are proposed.

## 2.4 Original Frame Strength Analysis

The traditional method to simulate steel plate spring suspension to analyse the strength of the frame is to add the steel plate spring simulation unit in finite element software like HyperMesh. Constraints are applied at the wheels, and the load size of the frame-carrying parts is imposed under various working conditions for simulation and analysis.

To simulate steel plate spring suspension, a CBUSH unit can be added at the suspension support. Its vertical stiffness is set to match the stiffness of the steel plate spring. The two CBUSH units simulating the same set of leaf springs are connected to the height of the wheel centre, and the axle is simulated using the CBEAM unit. However, because the CBUSH unit can only simulate the vertical stiffness, it cannot accurately replicate the force and moment generated by the steel plate spring. Especially in torsional conditions, when the frame and leaf spring are greatly deformed, the moment on the leaf spring support cannot be generated using the CBUSH unit alone.

Alternatively, the curved structure can be assembled, and the unit material can be provided. The thickness of the unit can be adjusted, and the vertical load can be applied until the vertical stiffness matches the stiffness of the leaf spring. This is still similar in nature to the CBUSH cell and disregards the lugs in the leaf spring suspension system. This simulation method leads to additional stresses on both suspension supports as a result of the deformation of the cell, and the simulation results are biased.

In order to prevent deviation in the results of traditional finite element software simulations of steel plate spring suspension for analysing the strength of the frame, this study extracts the forces and moments at the suspension supports of the vehicle under typical working conditions using ADAMS/CAR software, and applies them to the finite element model of the frame. At the same time, the unconstrained boundary problem is solved by combining the inertia

release method, and the frame strength is analysed. The results obtained in this manner are more closely aligned with the actual conditions of the frame.

The loads applied to each load-carrying component of the frame are shown in Table 5. The cab and personnel assembly, power assembly, fuel tank, battery, and cargo box assembly are connected to the frame mounting points using concentrated loads based on their centre of mass positions. Although the mass of other components, such as the line piping, has less influence on the frame condition analysis, this mass is integrated with the cargo box assembly as one part to ensure the accuracy of the mass on the spring. The self-weight of the frame is applied as a uniform load.

**Table 5** Loads on frame-carrying components

| Load assembly | Mass/kg |
|---|---|
| Cab and crew assembly | 541 |
| Powertrain | 537 |
| Fuel tank | 143 |
| Battery | 29 |
| Cargo boxes and cargo assemblies | 2,228 |

The inertial release method essentially calculates the acceleration of the model under the external force during the static analysis, and then converts the acceleration into an inertial force and applies it in the opposite direction, thus constructing an "equilibrium" force system. The nodes with zero displacements and reaction forces are called "virtual constraints", and the displacement cloud obtained from the solution describes the relative motion of each node with respect to the node of the support [16].

In analysing the strength of the present frame, if the loads at its load-bearing components and suspension mounts are applied to the frame at the same time without restraining the frame, it will not be possible to carry out the conventional finite element solution, but the inertia release method can be used to solve this kind of unconstrained problem effectively.

The procedure for evaluating the structural integrity of the frame using the inertial release method involves the following steps:

(1) Initially, HyperMesh software is utilised to extract the type and magnitude of the force acting on the tyre under various typical working conditions. Table 6 presents the limitations imposed on the tyres under various operational conditions, while Table 7 provides information on the types and intensities of loads exerted on the tyres.

**Table 6** Constrained degrees of freedom for each working condition

| Wheel centre position | Left front wheel | Right front wheel | Left rear wheel | Right rear wheel |
|---|---|---|---|---|
| Bending condition | X, Y, Z | X, Z | Y, Z | Z |
| Acceleration condition | Y, Z | Z | X, Y, Z | X, Z |
| Steering condition | X, Y, Z | Y, Z | Y, Z | Y, Z |
| Braking condition | X, Y, Z | X, Z | X, Y, Z | X, Z |
| Ex-torsion condition | X, Z=-100 mm | X, Y, Z | Z | Y, Z |
| Post-torsion condition | Z | Y, Z | X, Z=-100 mm | X, Y, Z |

**Table 7** Load types and magnitudes for each working condition

| Conditions | Type of load | Left front wheel/N | Right front wheel/N | Left rear wheel/N | Right rear wheel/N |
|---|---|---|---|---|---|
| Bending condition | Z (Centre of wheel) | 8,221 | 8,424 | 10,050 | 10,700 |
| Acceleration condition | X (Centre of wheel) | 0 | 0 | -10,980 | -11,450 |
| | Z (Centre of wheel) | 8,479 | 8,796 | 18,090 | 19,070 |
| Steering condition | Y (Tyre grounding point) | 8,316 | 1,658 | 9,402 | 1,104 |
| | Z (Centre of wheel) | 12,100 | 4,543 | 17,150 | 3,599 |
| Braking condition | X (Tyre grounding point) | 8,812 | 8,813 | 5,782 | 4,637 |
| | Z (Centre of wheel) | 16,410 | 16,410 | 10,170 | 11,440 |
| Ex-Torsion condition | Z (Centre of wheel) | 14,170 | 8,450 | 10,860 | 17,650 |
| Post-Torsion condition | Z (Centre of wheel) | 8,069 | 14,550 | 16,750 | 11,760 |

(2) Subsequently, an ADAMS/CAR module is utilised to establish a model of steel plate spring suspension. The load data obtained from the previous analysis are then imported into the model to calculate the force exerted on the suspension support under different operational circumstances. In this case, we will consider the bending condition as an illustrative example. Table 8 presents the force exerted on the suspension support under bending conditions. The force analysis of the suspension support in other operational scenarios remains consistent with the analysis conducted in this particular case.

(3) Finally, the suspension support stresses and the loads on each load-bearing component of the frame are inputted into the HyperMesh frame model. The inertia release method is then employed to calculate the frame strength and determine the stresses of the original steel frame under different working conditions. These stresses are presented in Table 9.

**Table 8** Forces and moments of each suspension support under bending condition

| | FX/N | FY/N | FZ/N | TX/N·mm | TY/N·mm | TZ/N·mm |
|---|---|---|---|---|---|---|
| Front suspension left front strut | 1,743.09 | 44.12 | 3,828.72 | 8,392.53 | 230.86 | -476.57 |
| Front suspension left rear strut | -1,584.86 | -44.81 | 4,028.79 | 2,439.85 | -386.97 | -1,307.37 |
| Front suspension right front strut | 1,511.61 | 45.14 | 4,046.03 | 8,388.08 | -231.52 | -478.00 |
| Front suspension right rear strut | -1,669.84 | -44.45 | 4,199.51 | 2,468.51 | -661.10 | -1,308.80 |
| Rear suspension co-spring left front strut | -882.59 | 20.64 | 2,982.92 | 4,805.28 | 1,361.92 | -253.33 |
| Rear suspension co-spring left rear strut | -167.39 | -31.60 | 2,953.42 | 1,883.87 | -420.22 | -211.04 |
| Rear suspension co-spring right front strut | -709.28 | 20.86 | 3,327.87 | 4,811.09 | 924.52 | -260.00 |

| | FX/N | FY/N | FZ/N | TX/N·mm | TY/N·mm | TZ/N·mm |
|---|---|---|---|---|---|---|
| Rear suspension co-spring right rear strut | -159.61 | -31.83 | 3,300.75 | 1,897.94 | -327.89 | -203.26 |
| Rear suspension main spring left front strut | 1,271.40 | 35.77 | 1,383.59 | 5,282.41 | 742.19 | 6.47 |
| Rear suspension main spring left rear strut | -76.00 | -24.86 | 1,565.85 | 3,784.41 | -1,001.31 | -94.94 |
| Rear suspension main spring right front strut | 790.75 | 35.94 | 1,633.45 | 5,285.64 | 492.65 | 8.01 |
| Rear suspension main spring right rear strut | -67.29 | -24.91 | 1,762.96 | 3,770.92 | -678.72 | -102.45 |

**Table 9** Strength analysis of the frame under various working conditions

| Conditions | Maximum stress region | Maximum stress value/MPa | Calculation of safety factors |
|---|---|---|---|
| Bending condition | Powertrain lifting beam; Suspension mounts | 234.8 | 1.469 |
| Acceleration condition | Lower wing surface of longitudinal beam between two axles of the frame | 332.9 | 1.036 |
| Steering condition | Bend outer longitudinal beam; Crossbeam to longitudinal beam joints | 827.4 | 0.417 |
| Braking condition | Suspension mounts; Longitudinal beam area between front and rear suspension | 437.5 | 0.789 |
| Ex-torsion condition | Each main beam area; Crossbeam to longitudinal beam joint plate | 2,049 | 0.168 |
| Post-torsion condition | Each main beam area; Crossbeam to longitudinal beam joint plate | 1,645 | 0.210 |

The results of the frame strength calculation using the inertia release method, as presented in Table 9, indicate that only the strengths of bending and acceleration meet the specified requirements. However, the maximum stresses for the remaining four conditions exceed the yield strength of the material. Consequently, the calculated safety factor is less than 1, indicating that the frame does not meet the strength requirements under the corresponding working conditions. It is imperative to consider the strength specifications of these operational circumstances during the design process of aluminium alloy frames in forthcoming endeavours.

## 3. Aluminium Alloy Frame Topology Optimisation

In order to obtain an aluminium alloy frame that meets the performance requirements, this paper uses topology optimisation to find the optimal material distribution form of the aluminium alloy frame. The topology optimisation of this frame takes the volume fraction as the constraint, and the minimum flexibility under each working condition as the objective function. Based on the optimisation results, and combined with the requirements of the company and the characteristics of aluminium alloy forming, the aluminium alloy frame is designed.

### 3.1 Basic Theory and Applications of Topology Optimisation

The purpose of topology optimisation is to find the optimal distribution of tubes and their optimal sizes for discrete structures or the optimal form of material distribution for continuum structures, in order to use the material most sparingly or to optimise the structural performance. Topology optimisation methods for continuum structures have been rapidly developed after the homogenization theory, mainly including the variable density method, asymptotic structure optimisation method, variable thickness method, homogenisation method and independent-continuous-mapping method [17]. In this paper, the topology optimisation method adopts the variable density method.

Common interpolation models in the variable density method are solid isotropic microstructures with penalisation (SIMP) and rational approximation of material properties (RAMP). Poisson's ratio in the SIMP model is constant, and a continuous variable $x_i$ is introduced that varies between [0 and 1], i.e., $0 \le x \le 1$. In order to make the density of each cell converge to 0 or 1, a penalty factor $p$ is introduced, which is set to $p > 1$, and there is a limited penalty for intermediate-density cells in order to reduce their number. The relational equation for the modulus of elasticity of the unit before and after optimisation is given by

$$E\left(x_i\right) = x_i^p E_0 \tag{3}$$

where $E\left(x_i\right)$ is the interpolated modulus of elasticity and $E_0$ is the modulus of elasticity of the actual material, while in order to prevent the singularity of the stiffness matrix, the minimum relative density $x_{\min}$ is set, which can be taken as the value of $x_{\min}$ =0.00001 so that

$$0 < x_{\min} \le x_i \le 1 \tag{4}$$

The mass of the optimised aluminium alloy frame should be lower than the mass of the original frame and should meet the stiffness-strength requirements. That is, under the condition of constraining a certain material volume, with the minimum structural flexibility as the goal, its topology optimisation mathematical model can be expressed as:

$$\begin{cases} Find: x = \left\{x_1, x_2, x_3, \cdots, x_n\right\}^T \\ \min: c = F^T U = U^T K U = \sum_{i=1}^{n} u_i^T k_i u_i \\ s.t.: KU = F \\ V^* = \sum_{i=1}^{n} x_i v_i \le fV \\ 0 < x_{\min} \le x_i \le 1 \end{cases} \tag{5}$$

where $n$ is the total number of cells in the design area, $c$ is the structural flexibility, $K$ denotes the stiffness matrix, $U$ denotes the displacement vector, $F$ denotes the load vector, $f$ is the fraction of the structural volume constrained, and $V$ is the design area volume.

### 3.2 Grounded Theory and the Application of the Exponential Scaling Hierarchical Analysis Approach

Because each working condition occurs differently in the actual driving process of the vehicle and has a different influence on the frame, the weight value of each working condition in the weighted flexibility of the objective function is also different. In the general design

process, only a qualitative judgement can be made on the weight assigned to each working condition, and it is impossible to accurately obtain the weight value of each working condition under multiple working conditions. In contrast, the exponential scale hierarchical analysis method can qualitatively and quantitatively analyse multiple working conditions, thus obtaining a more objective weight value for each working condition.

**Table 10** Meaning of each order index scale

| Scale | Meaning |
|---|---|
| d0 | The two factors are of equal importance compared to each other. |
| d2 | The former is slightly more important than the latter when the two factors are compared. |
| d4 | When the two factors are compared, the former is significantly more important than the latter. |
| d6 | The former is strongly more important than the latter when the two factors are compared. |
| d8 | The two factors are compared, with the former being extremely more important than the latter. |
| d1,d3,d5,d7 | Indicates the intermediate value of the above adjacent judgments. |
| Reciprocal | $a_{ji} = 1/a_{ij}$ |

**Table 11** Average randomized consistency indicators

| Exponential Scale Judgment Matrix Order | 1 | 2 | 3 | 4 | 5 | 6 | 7 | 8 | 9 |
|---|---|---|---|---|---|---|---|---|---|
| R.I. | 0 | 0 | 0.36 | 0.58 | 0.72 | 0.82 | 0.88 | 0.93 | 0.97 |

Hierarchical analysis is a kind of decision-making method that constructs a judgment matrix through two-by-two comparisons between different factors and conducts a consistency judgment to obtain relative weights. The construction method of the judgment matrix in hierarchical analysis is to compare the factors $C_i\left(i=1,2,\cdots,n\right)$ two by two and determine the relative weight value $a_{ij}\left(i=1,2,\cdots,n;\ j=1,2,\cdots,n\right)$ according to the degree of importance to obtain the judgment matrix $A=\left(a_{ij}\right)_{n\times n}\left(i=1,2,\cdots,n;\ j=1,2,\cdots,n\right)$.

The scaling method of $a_{ij}$ is generally a 1~9 scale, but the judgment matrix requires a comparison of the ratio of the importance of two factors, while the 1~9 scale indicates the difference between the importance of two factors, thus leading to the distortion of the calculation results of the relative weight. Besides, the consistency of the judgment matrix is not equal to the consistency of the judgment thinking. In this paper, the index scale method is used to construct the judgment matrix, and the resulting consistency of the judgment matrix coincides with the consistency of thinking. The construction ability of the consistency matrix is strong, and the weight ranking of each factor is consistent with the actual ranking results. The exponential scaling of the judgment matrix is defined as shown in Table 10, where $d=9^{1/8}=1.3161$.

Two-by-two comparisons are made for each of the above types of working conditions, and a judgment matrix $A$ is constructed based on the meanings of the scales in Table 10:

$$A=\begin{bmatrix} 1 & 9^{\frac{1}{4}} & 3 & 3 & 9^{\frac{3}{4}} & 9^{\frac{3}{4}} \\ 9^{-\frac{1}{4}} & 1 & 9^{\frac{1}{4}} & 9^{\frac{1}{4}} & 9^{\frac{3}{4}} & 9^{\frac{3}{4}} \\ \frac{1}{3} & 9^{-\frac{1}{4}} & 1 & 1 & 3 & 3 \\ \frac{1}{3} & 9^{-\frac{1}{4}} & 1 & 1 & 3 & 3 \\ 9^{-\frac{3}{4}} & 9^{-\frac{3}{4}} & \frac{1}{3} & \frac{1}{3} & 1 & 9^{\frac{1}{4}} \\ 9^{-\frac{3}{4}} & 9^{-\frac{3}{4}} & \frac{1}{3} & \frac{1}{3} & 9^{-\frac{1}{4}} & 1 \end{bmatrix} \tag{6}$$

The maximum eigenvalue $\lambda_{\max}=6.0848$ of this matrix is calculated and according to the consistency index $CI$ formula

$$CI=\frac{\lambda_{\max}-n}{n-1} \tag{7}$$

The consistency ratio $CR$ is calculated by combining the average stochastic consistency index R.I. of the matrices of each order under the exponential scale shown in Table 11:

$$CR=\frac{CI}{RI} \tag{8}$$

The consistency ratio $CR=0.0207<0.1$ is obtained, so the consistency of the judgment matrix is considered acceptable.

The summation method is used to normalise the elements of $A$ by columns then the elements of the columns are added and the resulting vector is divided by the order 6 of $A$ to obtain the weight vector $W$, i.e.:

$$W_i=\frac{1}{n}\sum_{j=1}^{n}\frac{a_{ij}}{\sum_{k=1}^{n}a_{kj}},i=1,2,\cdots,n \tag{9}$$

**Table 12** Weight values for each working condition

| Conditions | Bending condition | Acceleration condition | Ex-torsion condition | Post-torsion condition | Braking condition | Steering condition |
|---|---|---|---|---|---|---|
| Weight value | 0.3596 | 0.2471 | 0.1427 | 0.1427 | 0.0591 | 0.0488 |

The weight vector $W=\left[0.3596 \quad 0.2471 \quad 0.1427 \quad 0.1427 \quad 0.0591 \quad 0.0488\right]^T$ is obtained. The weight values for the six working conditions are obtained by calculation as shown in Table 12.

## 3.3 Topology Optimisation Results

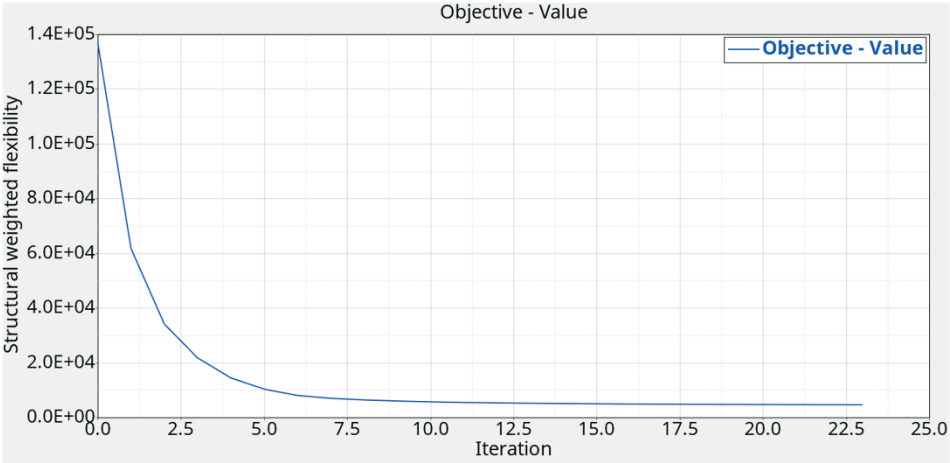


**Fig. 4** Structural weighted flexibility number of iterations plot

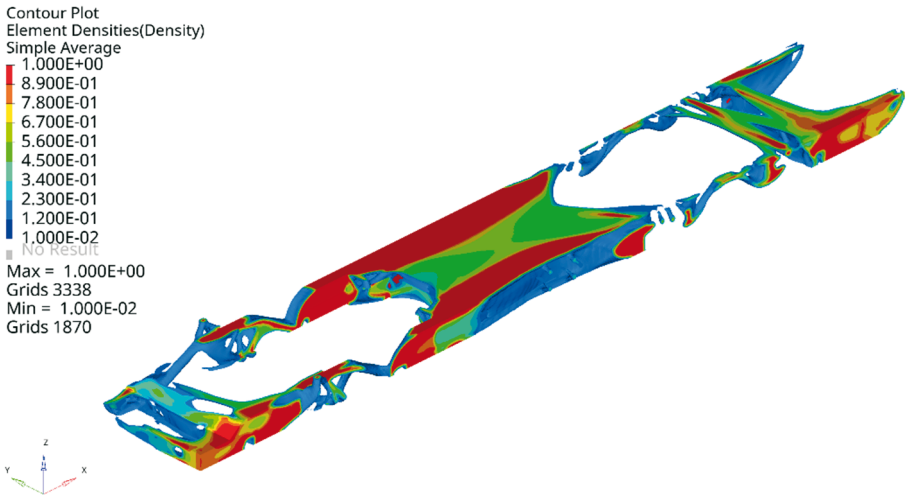


**Fig. 5** Topology optimisation result

Topology optimisation calculations were conducted utilising HyperMesh software. The convergence of the objective function is observed after 23 iterations. The relationship between the topology optimised structural weighted flexibility and the number of iterations is depicted in Fig. 4. The distribution of unit density in the topology optimisation results ranges from 0 to 1. A value closer to 1 indicates the greater importance of the unit for the strength of the frame. By adjusting the threshold, the optimal material distribution form of the aluminium alloy frame, as depicted in Fig. 5, can be obtained.

According to the results of topology optimisation, it can be seen that the installation of suspension and load bearing parts is more important, the longitudinal beam part between the front and rear suspension of the frame needs more structural support, and the material flow area corresponds basically to the area with higher stress in the strength analysis. The design of the aluminium alloy frame should follow the above results.

## 3.4 Aluminium Alloy Frame Design

The topology optimisation results provide important guidance for the design of the aluminium alloy frames. In addition, the product design should follow the production rules and requirements. For the consideration of cost control in the pre-production stage, the frame parts,

such as the longitudinal beams, cross beams and their connecting plates, should be produced by extrusion moulding. Three-dimensional modelling software UG is used to design the frame model.

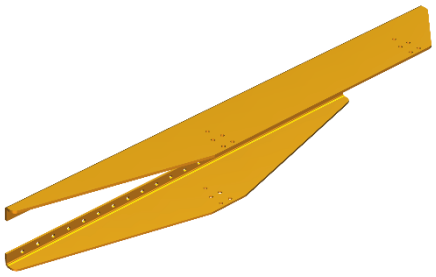

**Fig. 6** Connection plate model

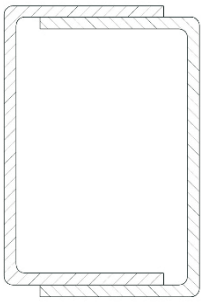

**Fig. 7** Cross-section of composite crossbeam

**Fig. 8** Aluminium alloy frame model

The upper and lower connecting plates of the cross member and longitudinal beam between the front and rear suspension are shown in Fig. 6. Their cross-sectional dimensions are the same and can be obtained by extrusion production from the same mould. The composite cross member connected by the above connecting plate adopts two cross members of the same size, and the installation method is shown in Fig. 7, so the same mould can be used. In addition, the last three main beams can also be produced by the same mould, thereby reducing the mould cost and processing cost.

For other non-regular parts, such as suspension mounts as important strength parts, the extrusion moulding method can hardly provide sufficient strength and cannot meet the spatial arrangement, so it can be replaced by the die-casting moulding method. The three-dimensional modelling software UG is used to design the frame model. The final aluminium alloy frame model is shown in Fig. 8.

## 4. Aluminium Alloy Frame Performance Calibration

In this section, the free modal state, bending stiffness, torsional stiffness, and strength of the aluminium alloy frame for each operating condition are examined using the same analytical methods as those used for the original steel frame. The mass of the aluminium alloy frame is calculated and compared with the mass of the original steel frame. The material properties of the aluminium alloy frame are shown in Table 13.

**Table 13** Properties of Al6061-T6 material

| Material | Modulus of elasticity/(N/m$^2$) | Poisson ratio | Density/(kg/m$^3$) | Shear modulus/(N/m$^2$) | Yield strength/(N/m$^2$) |
|---|---|---|---|---|---|
| Al6061-T6 | 6.90E+10 | 0.33 | 2.7E+3 | 2.6E+10 | 2.75E+8 |

**Table 14** Aluminium Alloy Frame Performance Benchmarking

| | Aluminium alloy frame | Performance indicators |
|---|---|---|
| First-order intrinsic frequency/Hz | 12.46 | >10 |
| Other intrinsic frequencies | Conformity | Avoiding the engine idling frequency of 25 Hz |
| Bending stiffness/(N/mm) | 1,254.71 | >1,055.41 |
| Torsional stiffness/(N·mm/°) | 496,604.83 | >198,373.87 |

The free modal, bending and torsional stiffnesses of the aluminium alloy frame were calculated, and the relevant performance parameters were summarised, as shown in Table 14.

The first-order free modal frequency of the aluminium alloy frame is 12.46 Hz, which is higher than that of the steel frame, and there is a gap between the excitation frequency and the road surface so that it will not resonate with the road surface, which is in line with the requirements of dynamic characteristics. The bending stiffness of the aluminium alloy frame is increased by 18.9% and the torsional stiffness by 150.3% compared with the original frame. The stiffness performance of the aluminium alloy frame is significantly stronger than that of the original steel frame.

**Table 15** Comparison of safety factors and quality

| | Aluminium alloy frame | Original steel frame |
|---|---|---|
| Factor of safety for bending condition | 2.683 | 1.469 |
| Factor of safety for accelerating condition | 1.439 | 1.036 |
| Factor of safety for steering condition | 1.015 | 0.417 |
| Factor of safety for braking condition | 1.516 | 0.789 |
| Factor of safety for torsion of front axle | 1.52 | <1 |
| Factor of safety for torsion of rear axle | 1.352 | <1 |
| Mass/kg | 157 | 226.9 |

The safety factors of the strength analysis of the aluminium alloy frame are compared with the original steel frame under various working conditions, and the mass of the two frames respectively is calculated, as summarised in Table 15.

The original steel frame has insufficient strength under the steering, braking, front axle torsion, and rear axle torsion conditions. Through the typical working condition analysis of the aluminium alloy frame under the same boundary conditions as the original steel frame, it can be seen that the aluminium alloy frame can meet the strength requirements under each working condition, and the strengthening of the corresponding parts of the aluminium alloy frame plays an important role.

After calculation, the mass of the original steel frame is 226.9 kg, and the mass of the designed aluminium alloy frame is 157 kg, which is 30.8% less than the mass of the original frame, and the lightweight effect is remarkable.

## 5. Conclusion

In this paper, an analysis was conducted on the dynamic and static characteristics of a steel frame in a light-duty truck, with a focus on the steel frame itself. We propose a multi-case topology optimisation method with weight coefficients for the design of an aluminium alloy

frame. The method is based on the exponential scale hierarchical analysis approach and aims to meet the performance and strength requirements of the frame.

(1) A finite element model was generated through the discretisation of the original steel frame. Subsequently, a free modal analysis was conducted to determine the bending stiffness and torsional stiffness of the frame. Additionally, this analysis was used to establish performance benchmarking indices for the aluminium alloy frame.

(2) ADAMS/CAR software was utilised to establish the suspension model, extract more accurate frame loads under typical operational conditions, and subsequently apply them to the frame in conjunction with the loads exerted by the frame-carrying components. In the context of the unconstrained scenario where loads are applied to the frame, the inertia release method was employed to assess the structural integrity of the frame under normal operating conditions. The findings indicate that the initial steel frame fails to meet the strength criteria when subjected to different operational circumstances, including steering, braking, front axle torsion, and rear axle torsion.

(3) The topology optimisation design of the designated region was conducted by imposing a constraint on the volume fraction and minimising the structural weighted flexibility. Given that the frame's working conditions share similar boundary conditions, but differ in frequency, the weight value for each working condition was determined using the exponential scale hierarchical analysis method. These weight values were then utilised in the weighted flexibility response of topology optimisation. After 23 iterations, the topology optimisation results were obtained. According to the results of topology optimisation and the specific requirements, a model of an aluminium alloy frame was designed.

(4) The aluminium alloy frame underwent both dynamic and static analyses, similar to those conducted for the steel frame. The first-order natural frequency of the optimised frame was enhanced significantly, ensuring a considerable distance from the excitation frequency of the road surface. Additionally, the other inherent frequencies were carefully adjusted to effectively avoid the engine idling frequency. As a result, the dynamic characteristics of the frame now meet the specified requirements. The calculated frame bending stiffness and torsional stiffness exhibit improvements when compared to the original frame. The safety coefficient of the strength of the aluminium alloy frame under each working condition is found to be greater than 1, indicating that it satisfies the strength requirements. The mass of the designed aluminium alloy frame is 157 kg, representing a reduction of 30.8% compared to the original steel frame. This significant decrease in weight demonstrates the remarkable lightweight effect achieved.

## REFERENCES

[1] Chen, R. Structural optimization and programming of thin-walled beam body skeleton with complex shape section. Jilin University 2020. https:/doi.org/10.27162/d.cnki.gjlin.2020.004705

[2] Khaple, S.; Golla, R. B. Prasad V. A review on the current status of Fe-Al based ferritic lightweight steel. Defence Technology 2023,26(08),1-22. https://doi.org/10.1016/j.dt.2022.11.019

[3] Francesco, P. D.; Lorenzo, B.; Andrea, A.; et al. Automotive lightweight design: simulation modelling of mass-related consumption for electric vehicles. Machines 2020,8(3),51. https://doi.org/10.3390/machines8030051

[4] Li, G.J.; Liu, X.L. A review of the current research status of automotive lightweighting technology. Materials Science and Technology 2020, 28(05):47-61.

[5] Lai, X.; Shi, J.Y.; Peng, T.Y.; et al. Research on variable density topology optimised adsorption structure for wall climbing robot. Mechanical Science and Technology 2021,40(06):821-827. https://doi.org/10.13433/j.cnki.1003-8728.20200336

[6] Wang, Z.Q. Lightweight design of an unmanned vehicle frame based on multi-working condition co-optimisation. Beijing Forestry University 2021. https://doi.org/10.26949/d.cnki.gblyu.2020.000297

[7] Li, Y.N.; Meng, D.; Zhang, Z.Y. Research on multi-condition topology optimization design of stainless steel spot welding vehicle considering weight coefficient. Journal of Physics: Conference Series 2022,2338(1). https://doi.org/10.1088/1742-6596/2338/1/012057

[8] Ma, F.W.; Wang, Z.J.; Yang, M.; et al. Research on the conceptual design method of lightweight automotive rear subframe. Automotive Engineering 2021,43(05):776-783+790. https://doi.org/10.19562/j.chinasae.qcgc.2021.05.018

[9] Ge, Y.; Liu, S.T. Evaluation of radar guide head jamming effectiveness based on exponentially scaled hierarchical analysis method and vague set. Journal of Detection and Control 2020,42(03):69-74.

[10] Tao, L.; Yang, J; Yang, Y; et al. A security risk assessment method for telematics based on situational awareness. Science Technology and Engineering 2022, 22(25):11113-11119.

[11] Gao, P. Study on risk assessment of debris flow based on index scale fuzzy analytic hierarchy process in Yinchanggou. Chengdu University of Technology 2023. https://doi.org/10.26986/d.cnki.gcdlc.2021.001272

[12] Sun, D.S.; Zhu, Y.; Zhou, S.X. Application of hierarchical analysis based on exponential scaling in bridge evaluation. Journal of Chongqing Jiaotong University (Natural Science Edition) 2010,29(06):867-870.

[13] Wang, H.; Gan, L. Analysis of Survivability of the Ship Propulsion System in a Severe Shock Environment, Based on the Fuzzy Theory and Analytic Hierarchy Process. Transactions of FAMENA 2023,47 (4),51-70. https://doi.org/10.21278/TOF.474044422

[14] Krstic, I.; et al. Aircraft performance checking process to achieve an acceptable level of safety through the compliance monitoring function. Transactions of FAMENA 2022,46 (1),57-80. https://doi.org/10.21278/TOF.461021620

[15] Zhou, J.C.; et al. Design optimization of a disc brake based on a multi-objective optimization algorithm and analytic hierarchy process method. Transactions of FAMENA 2018,42 (4),25-42. https://doi.org/10.21278/TOF.42403

[16] Sun, Y.B.; Dou, P.L. Overall strength analysis of floating wind turbine foundation with Truss Spar structure. Ship Science and Technology 2021,43(07):107-110.

[17] Zhang, L.; Xu, S.K.; Chen, J.; et al. Research progress on lightweight design of train body[J/OL]. Journal of Mechanical Engineering 1-20[2023-11-17]. https://doi.org/10.3901/JME.2023.24.177

Submitted: 18.11.2023

Accepted: 29.01.2024

Yang Zhou
Jiachuan Xu*
Weidong Qi
Xinyu Sun
Han Xu
School of Transportation and Vehicle Engineering, Shandong University of Technology, Zibo 255000, China
*Corresponding author:
xujc@sdut.edu.cn